Scientific
Research
Publishing

Influence of Continental Atmospheric Forcing on the Decadal Variability of the West African Monsoon

Adjoua Moïse Landry Famien[1,2]*, Sandrine Djakouré[2], Bi Tra Jean Claude Youan[3], Serge Janicot[4], Abé Delfin Ochou[2], Arona Diedhiou[5,6]

[1]Département des Sciences et Techniques, Université Alassane Ouattara de Bouaké, Bouaké, Côte d'Ivoire
[2]LASMES-UFR SSMT, Université Félix Houphouët Boigny d'Abidjan, Abidjan, Côte d'Ivoire
[3]LSS-UFR SSMT, Université Félix Houphouët Boigny d'Abidjan, Abidjan, Côte d'Ivoire
[4]Laboratoire d'Océanographie et du Climat: Expérimentations et Approches Numériques, Sorbonne Université, IRD, CNRS, MNHN, Paris, France
[5]Université Grenoble Alpes, IRD, CNRS, Grenoble INP, IGE, Grenoble, France
[6]UFHB-IRD Joint International Laboratory of Research on NEXUS Climate, Water, Energy and Agriculture and Development of Climate Services, African Centre of Excellence CCBAD (Climate Change, Biodiversity and Sustainable Agriculture), Université Félix Houphouët-Boigny, Abidjan, Cote D'Ivoire
Email: *famienmoise@uao.edu.ci, *famienmoise@gmail.com

Abstract

The West African Monsoon (WAM) is characterized by strong decadal and multi-decadal variability and the impacts can be catastrophic for the local populations. One of the factors put forward to explain this variability involves the role of atmospheric dynamics, linked in particular to the Saharan Heat Low (SHL). This article addresses this question by comparing the sets of preindustrial control and historical simulation data from climate models carried out in the framework of the CMIP5 project and observations data over the 20th century. Through multivariate statistical analyses, it was established that decadal modes of ocean variability and decadal variability of Saharan atmospheric dynamics significantly influence decadal variability of monsoon precipitation. These results also suggest the existence of external anthropogenic forcing, which is superimposed on the decadal natural variability inducing an intensification of the signal in the historical simulations compared to preindustrial control simulations. We have also shown that decadal rainfall variability in the Sahel, once the influence of oceanic modes has been eliminated, appears to be driven mainly by the activity of the Arabian Heat Low (AHL) in the central Sahel, and by the structure of the meridional temperature gradient over the inter-tropical Atlantic in the western Sahel.

1. Introduction

West Africa is a region whose rainfall is governed by the WAM [1]. The economies of the countries in this region are essentially based on agriculture and are therefore rainfall-dependent. So climate variations on various time scales have a considerable impact on the populations of this region. A number of studies have focused on variations on different spatiotemporal scales [1]-[6]. Most of them indicate a significant influence of sea surface temperatures (SST) on WAM. Others, however, show a role for the Saharan Heat Low (SHL) in response to the strong radiative heating received at the Earth's surface [7].

At the seasonal and intra-seasonal scales, the various studies carried out show that a strengthening of the SHL is associated with positive temperature anomalies in the lower layers, intensification of the monsoon flow, moisture advection over the central Sahel, intensification of the East African Jet and intensification of the vertical movements to the south of the ITCZ [4] [8] [9]. Ref. [8] through a modeling study clearly shows that the increase in temperature in the low-pressure area will increase its influence on the monsoon system through the strengthening of the temperature gradient between the Gulf of Guinea and the Sahara. Also, the interannual variability of the West African monsoon is strongly linked to surface temperature anomalies in the North Atlantic Ocean [2] [10] [11]. On decadal and multi-decadal scales, statistical analyses show that WAM variability is associated with the warm and cold phases of the Atlantic Multi-Decadal Oscillation (AMO) [5] [11] [12] [13] [14] [15], the Pacific Ocean Interdecadal Oscillation (IPO) [5] [14]. Several other studies suggest that the warm/cool phases of the AMO contribute to strengthening/weakening the Saharan thermal low [12] [16] [17] [18] [19].

Furthermore, [20] shows that the pattern of Sahelian rainfall recovery, following the drought of the 1980s, testifies to the fundamental, but not exclusive, role of SHL. Their work corroborates that of [21] on the role of greater heating over the Sahara in the last 30 years on Sahelian rainfall recovery. Ref. [10], in their work on the CMIP3 climate model ensemble, show that the intensification of SHL is correlated with Sahelian zone rainfall on interannual and multi-decadal time scales. They confirm the results of [20] on the causal role of SHL on Sahelian rainfall. Ref. [19] and [18] make an initial connection between the intensification of SHL and the AMO, without however putting forward a clear mechanism that could explain the link between the increase in North Atlantic SSTs and the intensification of SHL. Ref. [17] proposes a mechanism associating a cold phase in the SST of the extratropical North Atlantic Ocean and a reduc-

tion in Sahelian rainfall. This mechanism is governed by advection of cold air from Europe and North Africa amplified by a decrease in specific humidity, inducing a reduction in the greenhouse effect linked to water vapor, a weakening of the SST, and leading to a weakening of the WAM. Finally, [22] has addressed the representation of SHL in 22 CMIP5 climate models. Their work shows that SST variability cannot be the main cause of biases in the representation of SHL in models and suggests that they are linked to local mechanisms that control the evolution of SHL.

Although there are many studies concerning oceanic modes of decadal variability that may have an impact on West African rainfall, atmospheric processes linked to SHL may also be expressed on decadal and multi-decadal scales and have a potential impact on the decadal variability of these rains, and thus constitute an additional dynamic factor to be considered. Recent work has addressed the response of Sahelian rainfall to climate change [23]. In their work, the authors divide the precipitation response into two types: a rapid response associated with enhanced radiative forcing over the continent and the northern hemisphere relative to the southern hemisphere, and a slow response due to global changes in ocean circulation. They argue that rapid response outweighs slow response, and suggest international coordination of emission reduction efforts to mitigate rapid response. Consequently, understanding and assessing variations in continental atmospheric forcing are becoming issues of major importance. We therefore explore these issues in this study through the SHL, at decadal and multi-decadal time scales, and examine its influences on the WAM using CMIP5 simulations.

2. Data and Methods

2.1. Study Area

This research work is carried out in West Africa, which covers a vast area (3˚N-25˚N; 20˚W-20˚E), bounded to the south and west by the tropical Atlantic Ocean, to the north by the Sahara Desert and to the east by Chad and Cameroon (Figure 1). The West African region is characterized by a relatively flat relief with an average altitude of less than 500 meters. The plains occupy mainly the coastal edge and are drained by secondary rivers, with the exception of Senegal, Volta and Niger. Inland, low plateaus dominate. West Africa also boasts six mountain ranges with altitudes ranging from 1500 to 4000 meters: the Fouta Djalon (1515 meters) in the west, the Plateau de Jos (1830 meters) in the center-east, the Adamaoua massif (5000 meters) in the southeast and the Aïr massif (2020 meters), the Hoggar massif (2920 meters) and the Tibesti massif (3450 meters) in the north. These last two massifs lie on the northern edge of the West African region. The spatial development of these mountain ranges remains relatively low. Vegetation cover in West Africa is organized into more or less homogeneous zonal bands. From these zonal bands, we can distinguish three major land-use structures in West Africa: the forest zone located along the Guinean
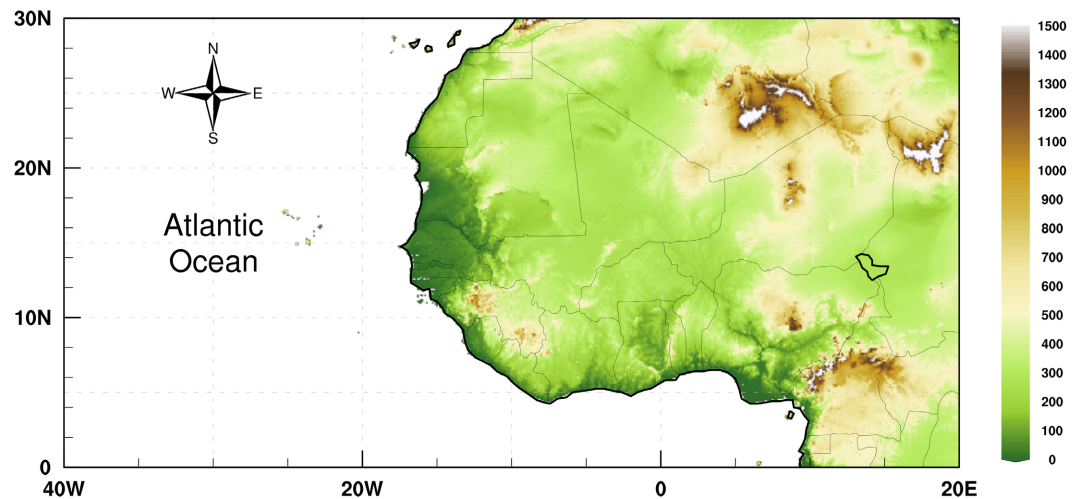
Figure 1. Topographical map of West Africa obtained from NOAA ETOPO 2022 topographic data (NOAA National Centers for Environmental Information. 2022: ETOPO 2022 15 Arc-Second Global Relief Model. NOAA National Centers for Environmental Information. https://doi.org/10.25921/fd45-gt74).

coast (<8°N), the arid zone located between 8°N and 13°N and the desert zone located beyond 13°N. This zonal organization of the vegetation cover is mainly controlled by the distribution of cumulative rainfall over the West African region. This region covers an area of over 6 million km^2, with a predominantly agricultural population. Seasonal patterns are governed by the West African monsoon system.

2.2. Data

2.2.1. Observations and Reanalysis Data

To analyze decadal rainfall variability in West Africa, we use version 3.21 of the CRU (Climate Research Unit) rainfall data covering all continents except Antarctica. This is a good-quality monthly dataset with fine spatial resolution (0.5° × 0.5°) and covers the period from 1901 to 2013 [24]. This version is an update of version 3.10 of the CRU data (https://crudata.uea.ac.uk/cru/data/hrg/). This database is used in a number of applications, including the evaluation of climate models and comparison with satellite products.

To characterize the decadal oceanic mode of variability, we used version 1 of the monthly Hadley Centre Sea Ice and Sea Surface Temperature data set (HadISST), available at https://www.metoffice.gov.uk/hadobs/hadisst/. This data covers the period from 1871 to 2013 [25] and has a spatial resolution of 1° × 1°. It is a dataset reconstructed using the RSOI (Reduced Space Optimal Interpolation) mesh method. We used this ocean surface temperature dataset to calculate the main decadal ocean variability modes corresponding to the global warming trend, the AMO, the Pacific Inter-decadal Oscillation (IPO) and the Indian Ocean Decadal Variability (IDV).

To obtain information on atmospheric circulation (in terms of structure and mechanisms), reanalysis data are essential. Atmospheric reanalyses are simulations of a numerical short-term weather forecasting model, based on assimilated

satellite data and in situ observations. They are physically consistent due to the use of a dynamic model, and more realistic than a pure simulation due to the use of assimilated data, which limits the biases of the model used. For this work, we use ERA-20CM data from the European Centre for Medium-Range Weather Forecasts (ECMWF). ERA-20CM is a dataset built as part of the European ERA-CLIM project

(https://www.ecmwf.int/en/forecasts/datasets/browse-reanalysis-datasets). It covers the period from 1899 to 2010. This database has a horizontal spectral resolution of T159 corresponding to approximately 125 km with 91 pressure levels ranging from the surface to 1 hPa [26]. As with most of the European Center's datasets, ERA-20CM is based on ECMWF's IFS2 (Integrated Forecasting System) atmospheric model (cycle Cy38r1), which has been configured to receive HadISST data as input and forcings as recommended by CMIP5. The ERA-20CM base is derived from AMIP-type experiments and was built according to the ten HadISST2.1 [27] SST and sea ice cover realizations prescribed by the Met Office Hadley Center, whose variability is closer to that of the observation sources on which it is based.

2.2.2. CMIP5 Dataset

For this work, we used monthly data from 29 climate models used in the CMIP5 project to analyze the variability of West African monsoons. Table 1 shows the 29 models used for simulation. Details of these models and the CMIP5 project experiments are contained in [28]. Two types of simulations were used: pre-industrial control simulations (piControl), which are simulations carried out over very long periods where the concentration of greenhouse gases (GHGs), aerosols, ozone and solar radiation have been fixed (constant) at their pre-industrial (1850) levels, and historical simulations (historical) available over the period 1850 to 2005 and incorporating the evolution over time of external forcing data.

2.3. Methods

A set of statistical processing has been performed to analyze the decadal and multi-decadal variability of continental atmospheric forcing over West Africa. Before proceeding with the various calculations, we interpolated all datasets to a regular 2° × 2° grid in order to facilitate the comparison of models with observations.

2.3.1. Definition of AMO, IPO and IDV Indexes

The decadal ocean modes (AMO, IPO and IDV) we analyze in this work are well-known and described in several works as the main decadal and multi-decadal variability modes [5] [29] [30] [31] [32]. Indeed, once the SSTs anomalies had been calculated, we used a 10th-order Butterworth low-pass filter with a cut-off period of 10 years with processing conditions at the ends of the series [33] and eliminated fluctuations linked to global warming by subtracting the linear trend. The dominant modes of variability were obtained from a Principal Component

Table 1. List of CMIP5 models used for pre-industrial control simulations and historical simulations.

Modèles CMIP5	Grid (lat × lon)	Modeling center
ACCESS1-0	1.25˚ × 1.875˚	Commonwealth Scientific and Industrial Research Organization (CSIRO)-Bureau of Meteorology (BOM); Australia
ACCESS1-3	1.25˚ × 1.875˚	
bcc-csm1-1	1.875˚ × 1.875˚	Beijing Climate Center (BCC); China
bcc-csm1-1-m	1.875˚ × 1.875˚	
BNU-ESM	2.81˚ × 2.81˚	Global Change and Earth System Science (GCESS); China
CanESM2	2.790 × 2.812	Canadian Centre for Climate Modelling and Analysis (CCCMA); Canada
CCSM4	1.9 × 2.5	Community Climate System Model version 4; Usa
CMCC-CESM	3.443 × 3.75	Centro Euro-Mediterraneo per I Cambiamenti Climatici (CMCC); Italy
CMCC-CMS	3.7111 × 3.75	
CNRM-CM5	1.4˚ × 1.4˚	Centre National de Recherches Météorologiques-Centre Européen de Recherche et de Formation Avancée en Calcul Scientifique (CNRM-CERFACS); France
CNRM-CM5-2	1.4˚ × 1.4˚	
CSIRO-Mk3-6-0	1.875˚ × 1.875˚	CSIRO-Queensland Climate Change Centre of Excellence (QCCE); Australia
FGOALS-g2	2.8˚ × 2.8˚	Center for Earth System Science (CESS); China
FGOALS-s2	2.8˚ × 2.8˚	
FIO-ESM	2.875 × 2.875	First Institute of Oceanography Earth System Model; China
GISS-E2-H-CC	2 × 2.5	Nasa Goddard Institute for space studies; Usa
GISS-E2-R-CC	2 × 2.5	
HadGEM2-CC	1.25˚ × 1.875˚	Met Office Hadley Centre (MOHC); United Kingdom
IPSL-CM5A-LR	1.9˚ × 3.75˚	Institut Pierre-Simon Laplace (IPSL); France
IPSL-CM5A-MR	1.25˚ × 2.5˚	
IPSL-CM5B-LR	1.9˚ × 3.75˚	
MIROC5	1.4˚ × 1.4˚	Model for Interdisciplinary Research on Climate (MIROC); Japan
MIROC-ESM	2.8125˚ × 2.8125˚	
MIROC-ESM-CHEM	2.8125˚ × 2.8125˚	
MPI-ESM-LR	1.875˚ × 1.875˚	Max Planck Institute for Meteorology (MPI-M); Germany
MPI-ESM-MR	1.875˚ × 1.875˚	
MPI-ESM-P	1.875˚ × 1.875˚	
NorESM1-M	1.875˚ × 2.5˚	Norwegian Climate Centre (NCC); Norway
NorESM1-ME	1.875˚ × 2.5˚	

Analysis (PCA) in which the first three modes were computed for each of the ocean basins. Thus, the Principal Components (PCs) of the first dominant modes of variability were used to characterize the AMO, IPO and IDV index.

2.3.2. Definition of SHL and AHL Indexes

Many studies used method based on the low-level atmospheric thickness (LLAT) to determine the location and the strength of the SHL ([4] [22] [34] [35]). To characterize the SHL index, our study follows also the work of [4] which concludes that the depression area evolves with the ITCZ displacement to reach a stable position during the summer over the Sahara and stipulates that LLAT is proportional to the average temperature between 925hPa and 700hPa layers. Therefore, we choose for our analysis, a regional index that best characterizes the Saharan Heat Low. Thus, the SHL index used in this work is obtained from the geographical mean air temperature at 850 hPa over the 7˚W-5˚E; 20˚N-30˚N domain.

We also focused on the East of SHL on the extension of the Arabian Heat Low (AHL) over North Africa. In this area, the low-level cyclonic circulation drives south-westerly air advection and can, depending on the amplitude of its development, connect with the center of action identified at 15˚E and contribute to strengthening southwesterly monsoon winds and precipitation over the central Sahel. Very few works have explored this point, the role of the DTS being mostly put forward. Ref. [36] analyzed this circulation structure and highlighted the strengthening of the AHL in summer and its impact in terms of a vertical zonal circulation structure associating mean lift over Arabia and mean subsidence over Libya. Therefore, after various tests, we choose, following the example of the SHL, an index that we conveniently call AHL, by the geographical average of the air temperature at 850 hPa over the domain 25˚E-35˚E; 18˚N-30˚N.

As with the oceanic decadal modes, the multi-decadal SHL and AHL signals was obtained from air temperature anomalies calculated and filtered using a 10th-order Butterworth low-pass filter with a cut-off period of 10 years and processing conditions at the ends of the series [33]. The influence of SHL and AHL on the West African monsoon was explored using regression maps on precipitation, 2 meters temperature, wind fields, specific humidity and geopotential height.

3. Results and Discussion

3.1. Influence of SHL on WAM at Decadal Scale in Control Simulations

3.1.1. Response in Precipitation

Figure 2 shows the regression maps of precipitation anomalies filtered at decadal scales on the decadal SHL index for the 29 CMIP5 models and for observations (top left). On this figure, the 2 meters temperature regression fields on SHL index have been superimposed in red contours. In the observations, the intensification of SHL induces an increase in temperature over the Saharan region and an increase in precipitation over the central and eastern Sahel, with a decrease in precipitation along the Guinean coast. The temperature response in the models is relatively well reproduced but with different forms.
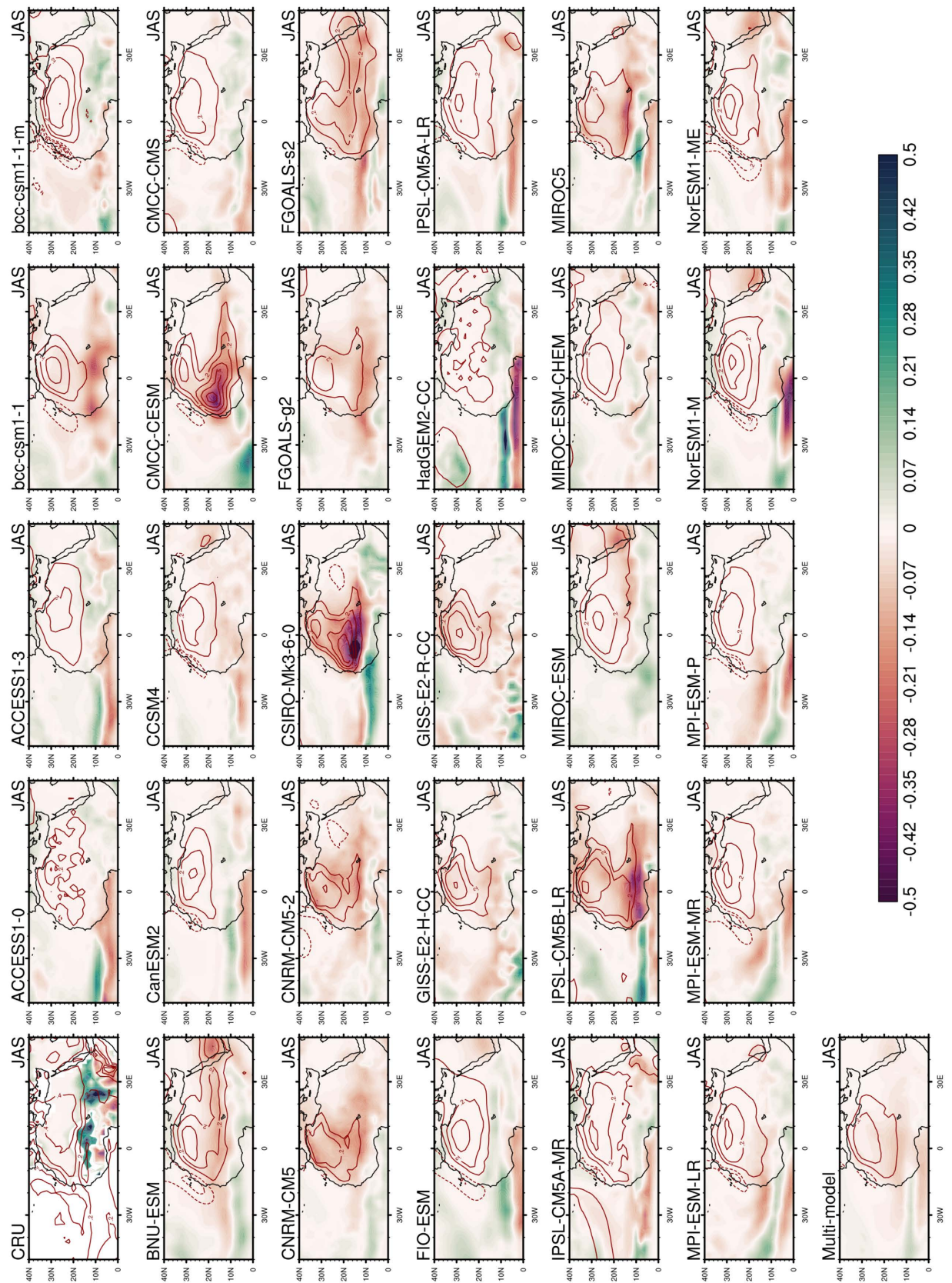
Figure 2. Regression maps of decadal anomalies of precipitation (colors) and 2 meters air temperature (red contours) on the SHL index for observational data, 29 CMIP5 models and the summer multi-model (JAS) in control simulations.

In most of the models, the structure of the SHL is characterized by temperature maxima between 20˚N and 30˚N. By contrast, in terms of precipitation, the inter-model dispersion is fairly wide. All models show a fairly weak response compared with observations. The multi-model mean obtained from 29 models shows a generalized decrease in precipitation over the entire West African region in response to an intensification of SHL. Over the ocean, the multi-model shows a band of positive precipitation anomalies around 10˚N, framed by negative anomalies on either side. Most of the models show negative precipitation anomalies over the continent in response to intensified SHL. These include bcc-csm1-1, BNU-ESM, CCSM4, CMCC-CESM, CNRM-CM5, CSIRO-MK3-6-0, IPSL-CM5B-LR and MPI-ESM-LR. For four of these models (bcc-csm1-1, CMCC-CESM, CSIRO-Mk3-6-0 and IPSL-CM5B-LR), the simulated response shows a significant decrease in precipitation over the Sahel, generally around 0.5 mm/day. Some of them show positive rainfall anomalies but are localized a little further south than observed. The CSIRO-Mk3-6-0 model, for example, reproduces an increase in rainfall along the Guinean coast. This is also the case for the MIROC5 model, whose positive structure extends as far east as Cameroon. In contrast, four models show positive precipitation structures: bcc-csm1-1-m, CanESM2, FIO-ESM and HadGEM2-CC reproduce positive precipitation anomalies over the eastern and central Sahel, as in the observations. Over the ocean, a large number of models show South/North precipitation dipoles: ACCESS1-0, ACCESS1-3, CanESM2, FIO-ESM, HadGEM2-CC and IPSL-CM5B-LR. However, for the BNU-ESM and CSIRO-Mk3-6-0 models, this dipole is reversed. In conclusion, the control simulations, viewed through the multi-model mean, produce a relationship between Sahelian precipitation and SHL which is very different, and even opposite to the relationship established in the observations.

3.1.2. Atmospheric Dynamics Associated

The same regressions were calculated from decadal geopotential height and wind at 925 hPa, sea-level pressure anomalies (Figure 3), and specific humidity at 925 hPa (Figure 4), in order to understand the mechanisms that explain the precipitation responses simulated in the models. The regression maps obtained show similarities with the structures obtained from observational data but also show clear differences between the models. In the observations, a warming of the SHL results in a strengthening of the cyclonic low-pressure circulation over the Sahara north of 20˚N, associated with increases in geopotential and pressure to the south, inducing a stronger meridional pressure gradient above 15˚N, and stronger monsoon winds in this same zone and weaker winds between 10˚N and the Guinean coast. This dynamic structure induces a strengthening of the meridional precipitation gradient, as shown in Figure 2, and is associated with strong humidification, with maximum values located between 10˚N and 20˚N (Figure 4). The multi-model mean shows, in response to an increase in temperatures of the SHL, and differently from observations, a very clear undulatory structure, with a cyclonic circulation, associated with negative geopotential and sea-level
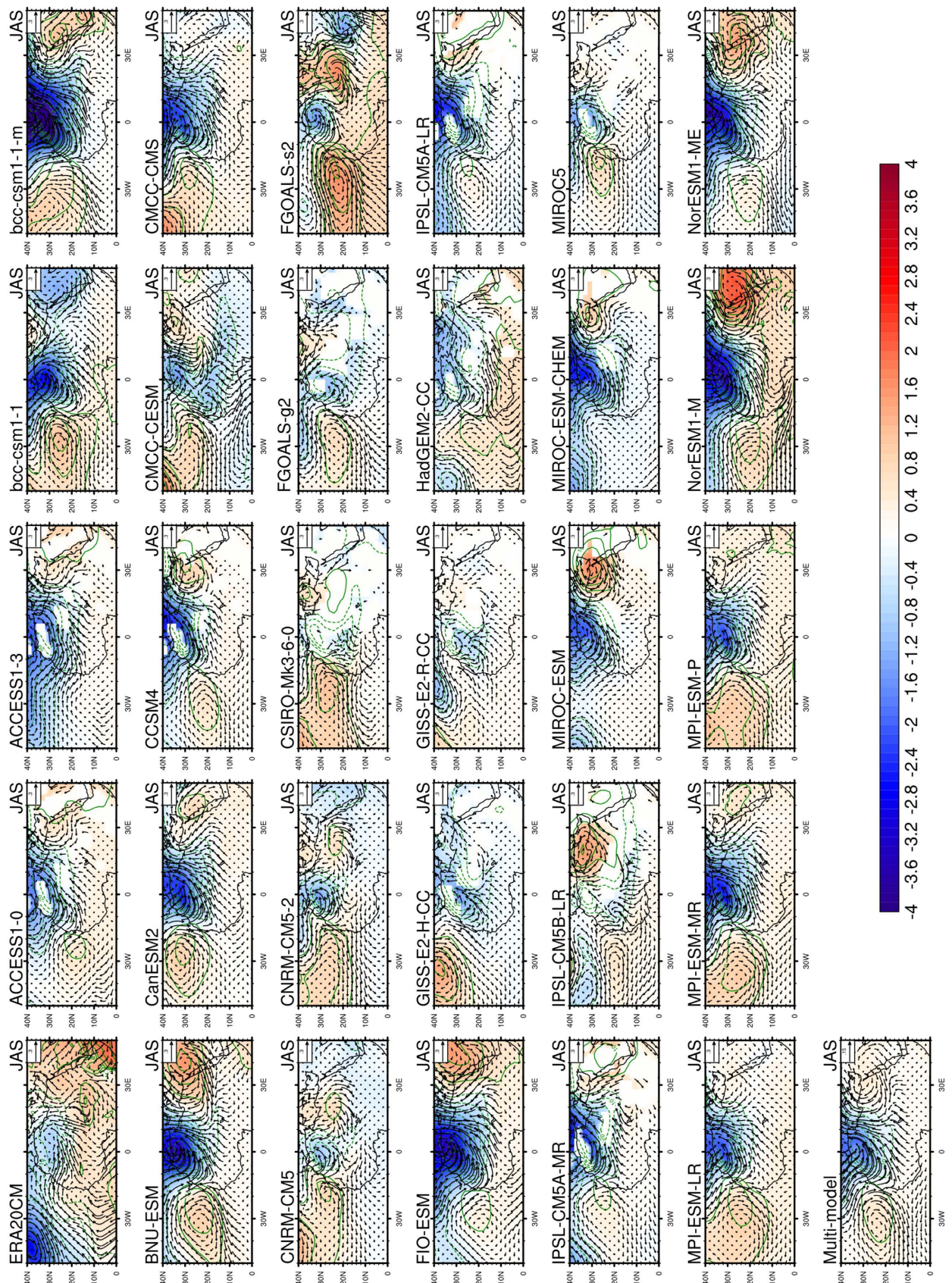
Figure 3. Same as **Figure 2**, but for sea level pressure (red contours), geopotential (colors) and wind fields (vectors) at 925 hPa.
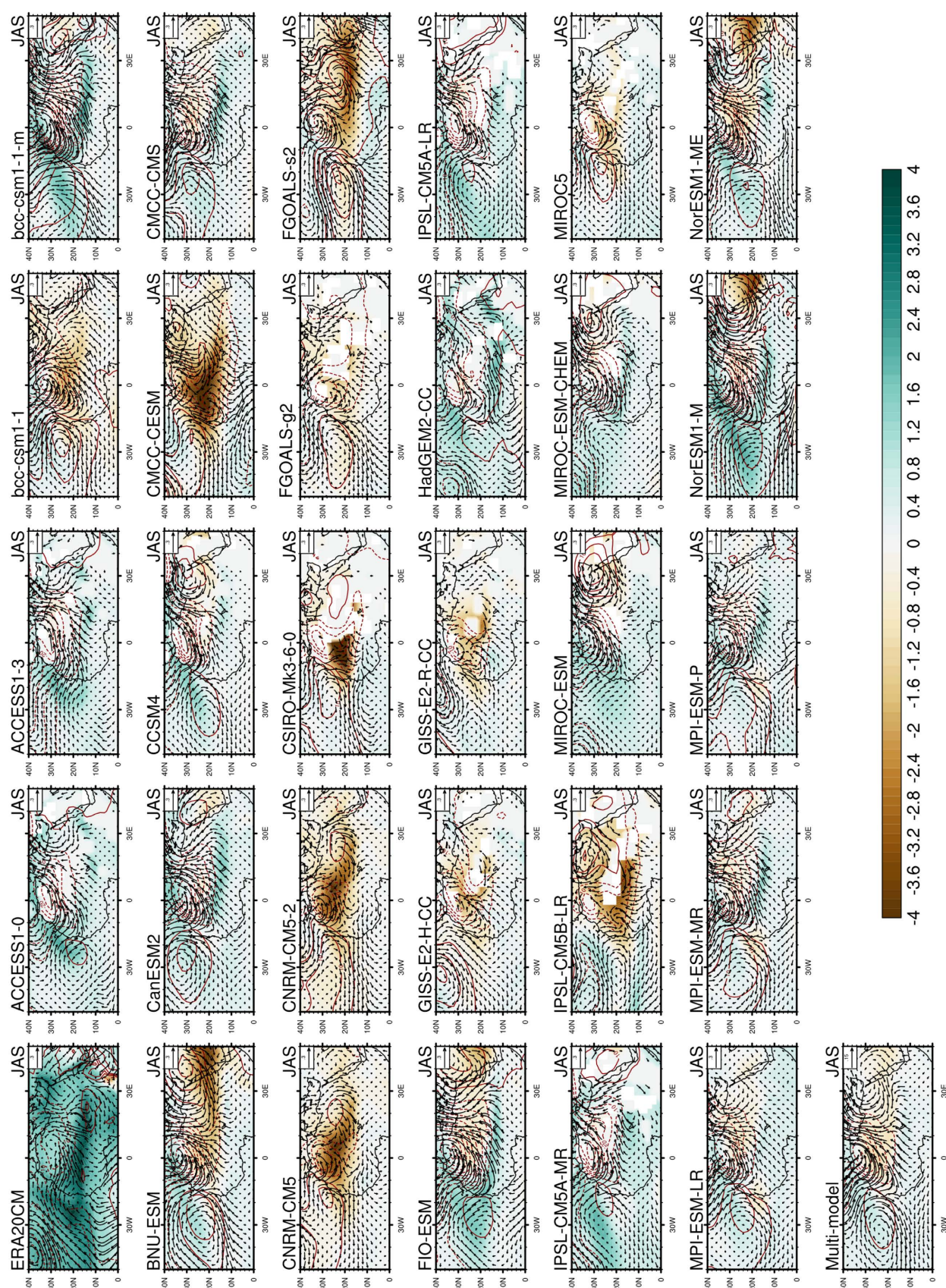
Figure 4. Same as **Figure 3**, but for specific humidity at 925 hPa (colors), sea level pressure (contours) and wind fields at 925 hPa.

pressure anomalies, centered on the meridian origin over the northern Sahara, and anticyclonic circulations located on either side. Cyclonic circulation induces a strengthening of south-westerly winds above 10˚N and a divergence of winds further south between 10˚N and the Guinean coast, leading to a modest but widespread drop in precipitation on the continent and a fall in specific humidity north of 15˚N, again in contradiction with observations. Furthermore, the easterly component of winds over the tropical Atlantic is reinforced by anticyclonic circulation (much less visible in observations), leading to a zone of convergence and higher precipitation.

Most models show negative geopotential anomalies localized in the low-pressure zone over the Sahara, with varying structures. Some models (bcc-csm1-1-m, BNU-ESM, FIO-ESM and NorESM1-M) show a fairly pronounced geopotential structure over the Sahara. Others, however, show rather weak signals: CSIRO-Mk3-6-0, GISS-E2-R-CC and IPSL-CM5B-LR. The CNRM-CM5, CNRM-CM5-2 and FGOALS-g2 models show areas of strong geopotentials on either side of the low-pressure zone over Morocco. The sea-level pressure regression fields superimposed on these maps are consistent with the geopotential structures. It should be noted at this point that the signals simulated by the models have higher absolute values than those from the reanalysis.

3.2. Influence of SHL and AHL on WAM Variability at Decadal-Scale in Historical Simulations

3.2.1. Influence of SHL

Here we examine the different responses in the case of historical simulations only on multi-model averages and in comparison, with control simulations and observations. As a reminder, the response structures in the control simulations showed a decrease in precipitation and drying north of 15˚N, in contradiction with the response structures in the observational data. Figure 5 shows regression maps derived from multi-model of decadal anomalies of precipitation (a-c), geopotential at 925 hPa (d-f) and specific humidity at 925 hPa (g-i) on the decadal SHL index for control, historical and observational simulations. The same types of structures were superimposed for 2-meter temperatures (contours in figures a-c), sea level pressure (contours in figures d-i) and wind fields at 925 hPa (vectors).

The multi-model mean from the historical simulations is generally close to control simulations for dynamics structures, and fairly close to observations for precipitation and specific humidity variables. In terms of atmospheric dynamics, the 2 meters temperature response and geopotential at 925 hPa of the historical multi-model mean shows very similar structures to those of the control simulations, with higher temperature values over the Sahara and a zone of low geopotentials over the Sahara with stronger weights (Figure 5e) than control simulations (Figure 5d) and observations (Figure 5f). The strengthening of the SHL is also accompanied by a decrease in sea-level pressure and a strengthening of cyclonic circulation, inducing stronger south-westerly winds on either side of 10˚N.
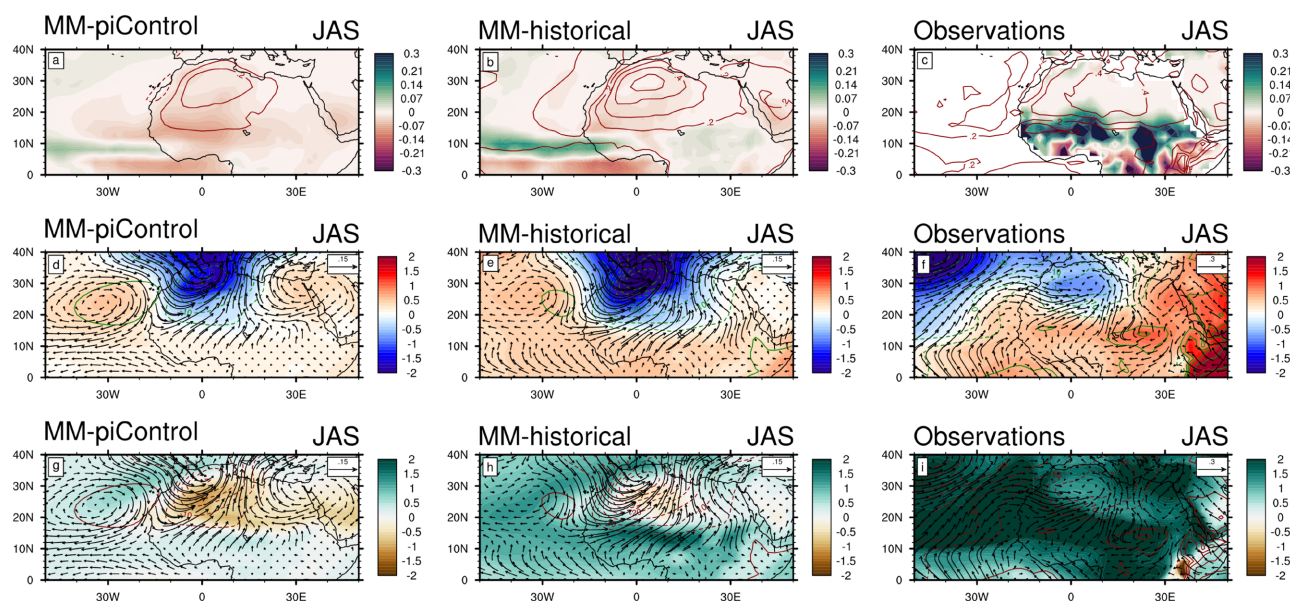
Figure 5. Regression maps on the decadal SHL index of decadal anomalies: (a-c) precipitation (colors) and 2 meters air temperature (red contours), (d-f) geopotential and wind fields at 925 hPa and sea-level pressure, (g-i) specific humidity and wind fields at 925 hPa, for observations and multi-model from pre-industrial control (MM-piControl) and historical (MM-historical) simulations. The precipitation color scale is different for observations.

Over the Atlantic Ocean, the anticyclonic circulation reproduced in the control simulations is also present, although a weaker intensity. In terms of humidity, the responses in the two types of simulations show strong similarities but remain different from those in the observational data. However, in the historical simulations, the humidity response shows more restricted negative humidity anomalies over the Sahara and much more extensive positive anomalies, which are closer to the structure of the observations. Finally, this multi-model mean correlatively presents a precipitation anomaly structure strongly similar to control simulations, but with more pronounced positive anomalies (**Figure 5b**), over both the continent and the tropical Atlantic Ocean. As in the control simulations, the structure derived from the historical simulations is quite different from that of the observations.

In **Figure 6**, we present the scatterplot of the mean of the regression coefficients on the decadal SHL index, 2 meters temperature anomalies taken over the depression zone (7˚W-5˚E; 20˚N-30˚N), precipitation over the North Sahel (SAHEL_N: 18˚W-10˚E; 16˚N-25˚N) and humidity over the North Sahel (SAHEL_N: 18˚W-10˚E; 16˚N-25˚N) and the South Sahel (SAHEL_S: 18˚W-10˚E; 10˚N-15˚N). The choice of areas is based on the homogeneity criterion of the regression structures analyzed above, for both control and historical simulations. This figure clearly shows a high degree of dispersion in the models. For a strengthening of the SHL, the majority of models show a decrease in rainfall over the northern Sahel in the control simulations. In historical simulations, the results are fairly mixed. More than half the models show a rainfall deficit, while just under a third show the opposite situation.

13
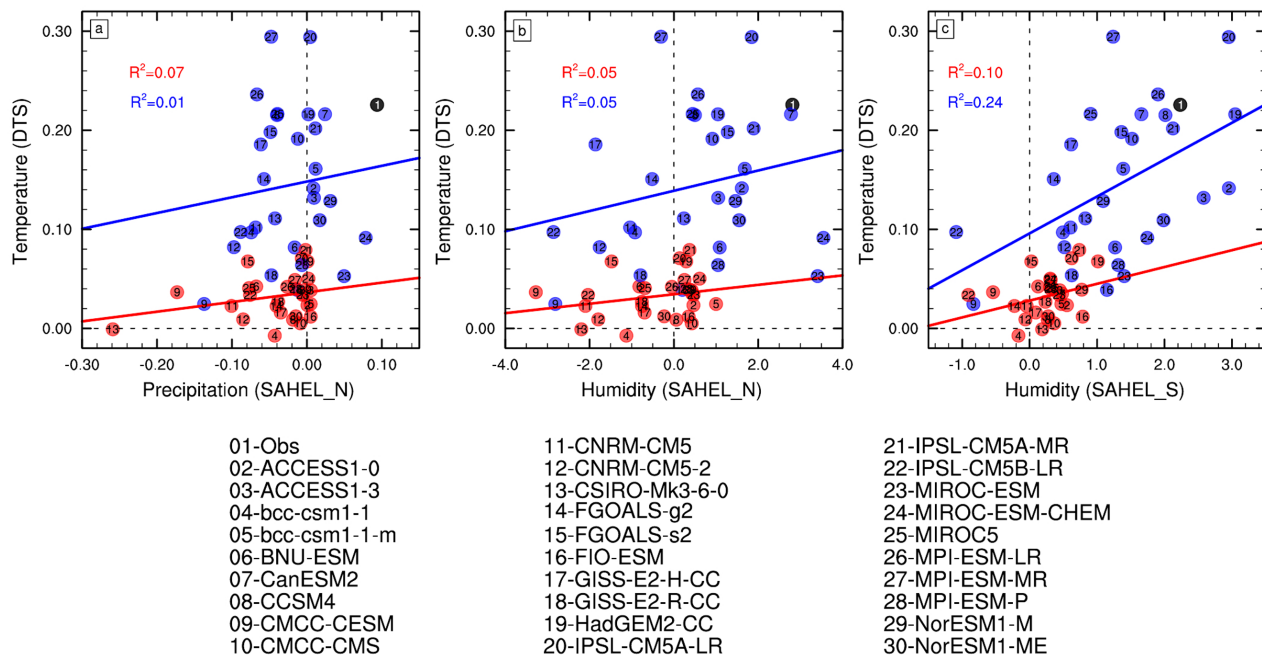
Figure 6. Scatterplots of regression coefficients on the SHL index of precipitation, specific humidity and 2 meters temperature anomalies averaged over the North Sahel (SAHEL_N: 18˚W-10˚E; 16˚N-25˚N), the Southern Sahel (SAHEL_S: 18˚W-10˚E; 10˚N-15˚N) and over the SHL domain (SHL: 7˚W-5˚E; 20˚N-30˚N) for each model in control simulations (red markers) and historical simulations (blue markers). The black dot represents the observations. The straight line represents the linear fit of these points.

In terms of sensitivity distribution, the linear correlations between these two variables are very weak. In terms of humidity in the northern Sahel, the situation is equally mixed. In the control simulations, the drying out observed in the multi-model is driven by half of the models showing high values of negative moisture anomalies (on average greater than $+2.0 \times 10^{-4}$ kg/kg per standard deviation) during an increase in SHL, while the other half reproduce anomalies on average equivalent to $+0.5 \times 10^{-4}$ kg/kg per standard deviation. However, in the historical simulations, a majority of models show positive moisture anomalies, leading to an attenuation of the drying of this region in the multi-model.

Analysis of Figure 6c shows that the deepening of the depression is more clearly associated with humidification of the Southern Sahel in most models for both types of simulation, with a better inter-model correlation in terms of sensitivity, particularly for historical simulations where a higher temperature anomaly of the SHL is associated with greater humidification over the Southern Sahel (the observation point being well inserted in this relationship).

Ref. [20] has suggested the existence of a positive feedback loop between temperature and water vapor over the Sahara: the observed increase in SHL temperature over the last 30 years has induced an intensification of water vapor convergence in the lower layers of the SHL, which causes an intensification of nocturnal surface heating by the greenhouse effect of this water vapor, and then, in turn, induces an increase in SHL temperature. In our results, this humidification linked to a warming of the SHL is found in observations, very little in historical

simulations and not at all in control simulations. It is correlatively associated with higher precipitation in the observations and to a lesser extent in the historical simulations, but not in the control simulations.

3.2.2. Influence of Arabian Heat Low (AHL)

Figure 7 presents the regression fields on the AHL decadal index of decadal anomalies for precipitation, 2 meters temperature, sea level pressure, geopotential, specific humidity and wind at 925 hPa. In the observations, the response structures corresponding to an increase in temperature in the AHL show an increase in precipitation over the Sahel, slightly stronger and more extensive than for the SHL (**Figure 5c**). This time, multi-model averages from control and historical simulations show strong similarities with observations. They reproduce well-developed positive temperature anomalies over the Sahara east of 0˚W (stronger for the historical simulations), associated with positive precipitation anomalies over West Africa with a stronger signal weight in the historical simulations, and a clear meridional dipole structure, reflecting a northward ascent of the ITCZ. These signals are globally reproduced in all models (not shown here). Geopotential responses correspond to a broad zone of low geopotential and negative pressure anomalies over the Sahara, clearly reproduced in the control and historical multi-model mean. This structure is stronger and more extensive than for the SHL, and drives a strengthening of westerly winds between 10˚N and 20˚N that extends from the Atlantic to the eastern Sahel (in particular the strengthening of the "low-level westerly jet" off Guinea analyzed by [37], and whose decadal variability is strongly correlated with that of Sahelian precipitation [38]. This also helps to understand the stronger signal of increased Sahelian precipitation relative to the AHL compared to the SHL. Here again, the signal is clearer in the historical simulation than in the control simulation, where westerly
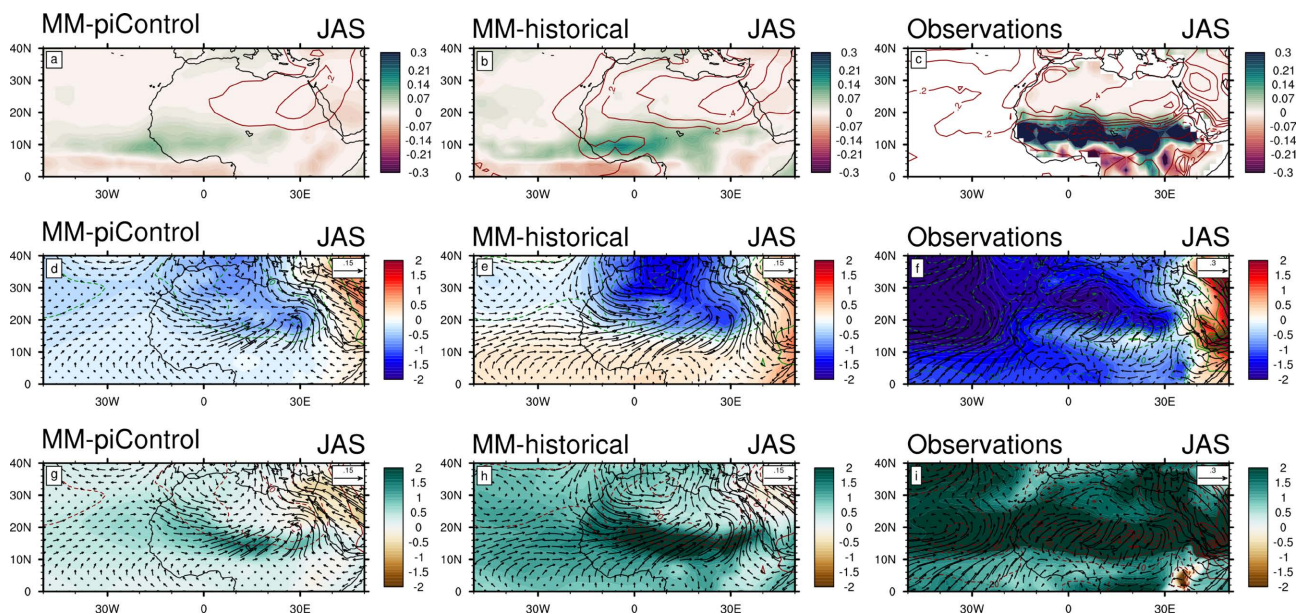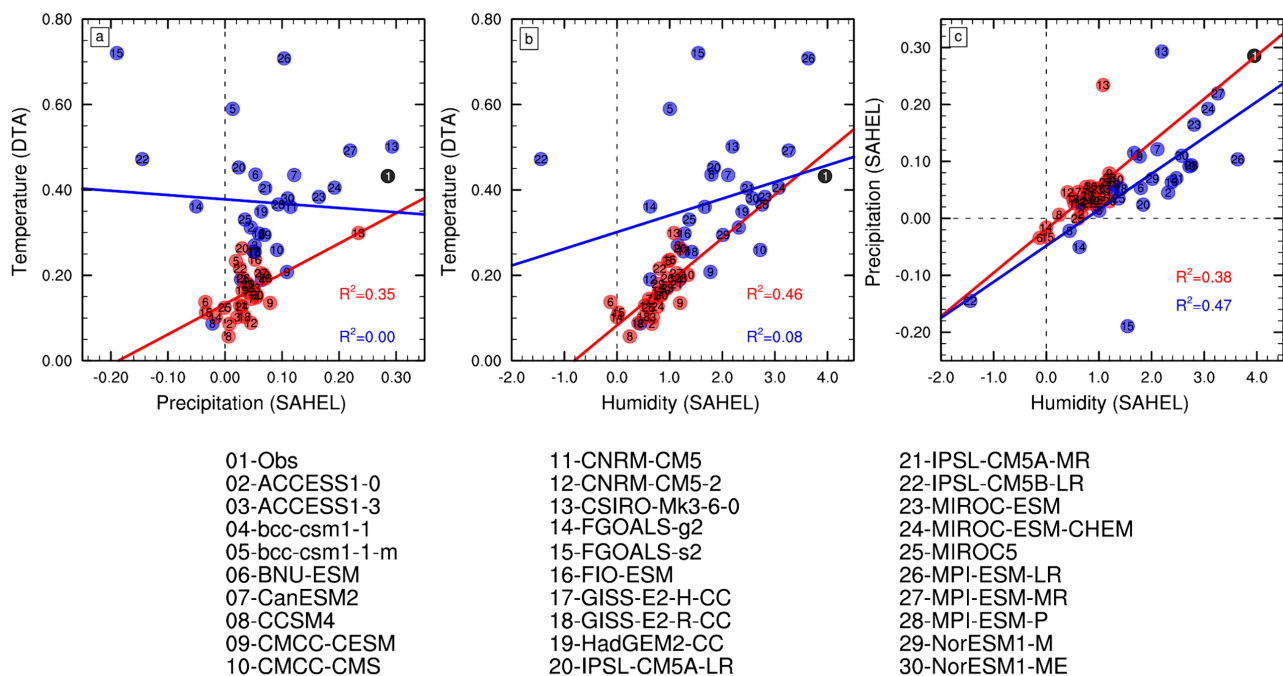

Figure 7. Same as **Figure 5** but for AHL index.

wind anomalies are limited over the continent. In terms of specific humidity, the results are consistent, with a more pronounced humidity surplus in the AHL and in the historical simulations. Finally, while these results are closer to the structures found in the observations, the fact remains that these structures in the observations have much stronger anomalies and a rather different spatial organization, particularly over the Atlantic.

Figure 8 shows the scatterplot of regression coefficients for precipitation anomalies, specific humidity on the AHL averaged over the Sahel (18˚W-10˚E; 10˚N-20˚N), and 2 meters temperature anomalies averaged over the AHL domain (25˚E-35˚E; 20˚N-30˚N) for each model (control simulations and historical simulations) and for observations. For a strengthening of the DTA, the individual models show a majority increase in Sahelian precipitation (Figure 8a), consistent with the rise in humidity (Figure 8b) over the Sahel in both control and historical simulations. Inter-model correlation in terms of rainfall or humidity sensitivity to a variation in AHL is fairly good in the control simulations, but very poor in the historical simulations.

3.3. Partials Regressions on the SHL and AHL Indexes

We analyzed the relationships between West African rainfall and the three oceanic modes (AMO, IPO, and IDV) on decadal timescales, as well as the SHL and AHL indexes in the observational data. Table 2 shows the intercorrelations between these indexes in summer over the period 1901-2005. The result confirms

01-Obs	11-CNRM-CM5	21-IPSL-CM5A-MR
02-ACCESS1-0	12-CNRM-CM5-2	22-IPSL-CM5B-LR
03-ACCESS1-3	13-CSIRO-Mk3-6-0	23-MIROC-ESM
04-bcc-csm1-1	14-FGOALS-g2	24-MIROC-ESM-CHEM
05-bcc-csm1-1-m	15-FGOALS-s2	25-MIROC5
06-BNU-ESM	16-FIO-ESM	26-MPI-ESM-LR
07-CanESM2	17-GISS-E2-H-CC	27-MPI-ESM-MR
08-CCSM4	18-GISS-E2-R-CC	28-MPI-ESM-P
09-CMCC-CESM	19-HadGEM2-CC	29-NorESM1-M
10-CMCC-CMS	20-IPSL-CM5A-LR	30-NorESM1-ME

Figure 8. Scatterplots of regression coefficients for precipitation, specific humidity and 2 meters temperature anomalies averaged over the Sahel (SAHEL: 18˚W-10˚E; 10˚N-20˚N) and the domain (AHL: 25˚E-35˚E; 20˚N-30˚N) for each model in control (red markers) and historical (blue markers) simulations. The black dot represents the observations. The straight line represents the linear fit of these points.

Table 2. Correlations over period from 1901-2005 between AMO, IPO, IDV, DTS and DTA decadal-scale indices in summer for observation data.

	AMO	IPO	IDV	SHL	AHL
AMO	1				
IPO	0.06	1			
IDV	0.05	0.44	1		
SHL	0.69	0.54	0.24	1	
AHL	0.85	0.09	0.01	0.69	1

on one hand, the non-correlation between AMO and the IPO and IDV modes, and on the other hand the fact that IPO and IDV have a certain dependence (correlation of +0.44). In this regard, we note the study by [39] showing the breakdown of this interrelation from the 2000s onwards, as a possible impact of global warming that is more noticeable on the Indian Ocean.

Continental atmospheric indices are correlated at +0.69 (50% shared variance). The SHL shows a strong correlation with the AMO (50% shared variance) and slightly weaker links with the IPO (30% variance) and negligible with the IDV. AHL has even stronger statistical links with AMO (70% variance) and negligible links with IPO and IDV. This analysis of correlations between low-pressure indices and the three decadal oceanic modes shows a probable dependence between SHL, AHL and AMO in observations. This suggests either a common evolution forced by an external factor or a possible forcing of AMO on the activity of SHL and AHL. Thus, [17] proposed a mechanism associating a cold phase in extratropical North Atlantic Ocean temperatures and a decrease in Sahelian rainfall via advections of cold air from Europe and North Africa amplified by a decrease in specific humidity inducing a reduction in the greenhouse effect linked to water vapor, a weakening of SHL, and leading to a weakening of the West African Monsoon.

In the following, in order to better distinguish the contribution of the depression indices from that of the AMO signal in the variability of WAM, we assume a probable dependence between the SHL, AHL and AMO, and we decompose the signal of each depression index into two signals (a signal due to the AMO and the residual signal) whose regression structures on the depression indices are analyzed below. Note that the results obtained by also eliminating the weight of the other two decadal ocean modes, IPO and IDV, give similar results, so we limit ourselves here to the elimination of the AMO signal.

3.3.1. Partial Regression on SHL Index

Intercorrelation scores between ocean modes also indicate intercorrelations with SHL and AHL indexes for control and historical simulations. In control simulations, correlations of SHL and AHL with AMO are very low, below 0.15 in absolute value (rising for some models to 0.20), whereas in historical simulations, correlations are higher, mostly between 0.2 and 0.4 in absolute value. In parallel,

SHL-AHL intercorrelations are variable, below 0.5 in the control simulations, and rising to 0.6 in the historical simulations, indicating a degree of mutual independence on a decadal scale.

To better understand the structural differences between simulations and observations, we compute the regression fields of the residual anomalies of precipitation, 2 meters temperature, sea level pressure, geopotential, specific humidity and wind fields at 925 hPa. The residual anomaly was obtained in several stages. First, at each grid point, we calculated the regression of the original anomalies on the AMO index. The regression coefficient obtained was then used to reconstruct anomalies (theoretical anomalies) due to AMO.

Finally, the residual was obtained by subtracting the theoretical anomalies obtained from the original anomalies. The regression structures of these residual anomalies on the residual SHL index are shown in **Figure 9**. Consistent with the low intercorrelations with the AMO, the responses obtained in the control multi-model simulation are similar to those obtained without subtraction of the AMO signal (see **Figure 5**). For the historical multi-model simulation, the structures are similar, but the overall amplitude of the signals is weakened. In particular, there is a weaker warm anomaly in the SHL domain, associated with a reduction in cyclonic circulation and an intensification of high geopotentials over the Atlantic Ocean, and a decrease in precipitation levels over both the continent and the tropical Atlantic Ocean, associated with a reduction in specific humidity values. However, the changes are much more marked in the observations, in line with the strong inter-correlations with AMO, particularly with a reversal in the sign of precipitation anomalies and a significant deficit in specific
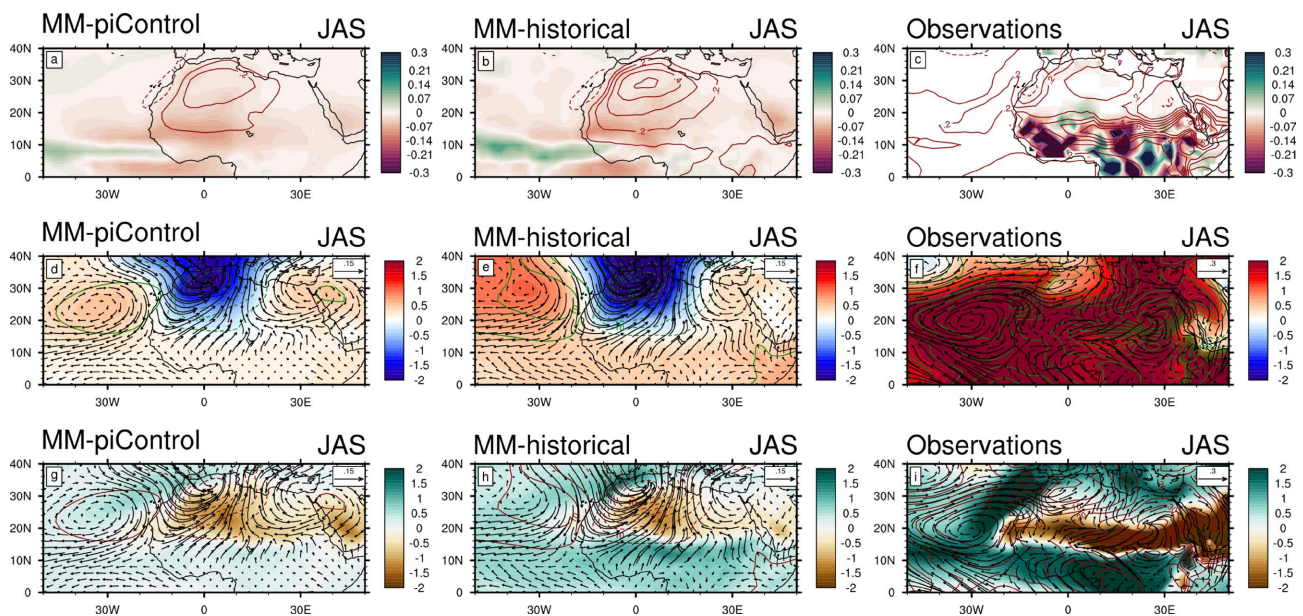
Figure 9. Regression maps on the decadal SHL index of decadal anomalies: (a-c) precipitation (colors) and 2 meters air temperature (red contours), (d-f) geopotential and wind fields at 925 hPa and sea level pressure, (g-i) specific humidity and wind fields at 925 hPa, after subtraction of AMO, for observations and multi-model averages from each of the simulations analyzed (control and historical simulations).
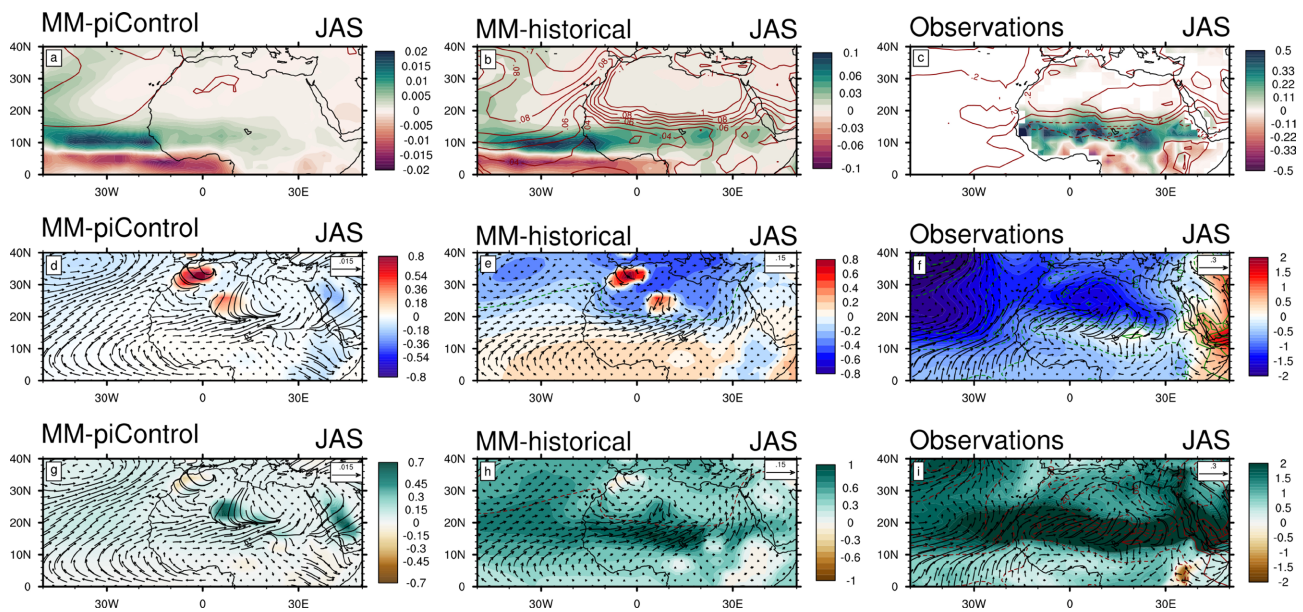
Figure 10. Regression maps on the decadal SHL index of decadal anomalies: (a-c) precipitation (colors) and 2 meters air temperature (red contours), (d-f) geopotential at 925 hPa, wind fields at 925 hPa and sea level pressure, (g-i) specific humidity at 925 hPa, wind fields at 925 hPa due to AMO for observations and multi-model averages from each of the simulations analysed (control and historical simulations).

humidity along the Sahelian strip. The circulation structure is also very similar to the simulations, particularly over the Atlantic Ocean. This reconciliation between the residual fields derived from observation and the control simulation, which is the reference in terms of internal climate variability, confirms the strong impact of AMO in the classic calculations of links between SHL and WAM published in the literature, and shows, once this influence has been eliminated, a loss of correlation or even anti-correlation between SHL activity and Sahelian precipitation.

Examination of the contribution of SHL signal due to AMO (Figure 10) shows the classic signal of an excess of precipitation and specific humidity over West Africa in both simulations, in agreement with observations, with, again, a stronger signal in the historical simulations than in the control simulations. This corresponds to a northward shift of the ITCZ visible over both the continent and the tropical Atlantic Ocean. This impact is also reflected in a sharp rise in temperature and associated cyclonic circulation over the Sahara.

This intensification is also accompanied by the AMO's direct oceanic footprint, which translates into a strengthening of the south-westerly winds that turn eastward off Senegal via the low-level westerly jet [37] and joins the westerly wind anomalies driven by the strengthening of SHL. Thus, in line with the study by [17], a positive phase of AMO induces a rise in temperatures over the Sahara and a deepening of SHL leading to a strengthening of rainfall in the Sahel. In conclusion, the direct relationship between SHL and Sahelian rainfall that is described in the multi-model control simulation is in fact largely dominated by the "external" influence of AMO over the historical period of observations. Similar

diagrams to Figure 6 have been produced, but are not shown due to their similar results.

3.3.2. Partial Regression on AHL Index

We produced similar analysis for the AHL index. The results are shown in Figure 11. As with SHL, the regression fields for the multi-model mean of the control simulations are very similar to those obtained without subtracting the effect of AMO. In the historical simulations, the signals are somewhat attenuated, but the positive regression between AHL intensity and West African rainfall is still high. These residual regression fields are very weak over the tropical Atlantic, and the impact of AHL on the cyclonic circulation that disappears over the ocean is moderately weakened over the continent. In the observations, on the other hand, the signals are extremely reduced by the removal of the AMO effect, with regression points now close to zero, consistent with the high correlation between AHL and AMO (+0.85). Analysis of the contribution of SHL signal due to AMO (not shown) shows structures similar to those obtained in Figure 10. Thus, the impact of AMO on the decadal variability of AHL and its relationship with WAM is even more marked than for SHL. Similar diagrams to Figure 8 have been produced, but are not shown due to their similar results.

3.4. Partial Regression on the Sahelian Precipitation Index

To investigate the links between the Saharan heat low and Sahelian precipitation at the decadal scale, we are developing a similar analysis, but using precipitation index and studying the associated regression fields, with and without the influence of oceanic modes. Highlighting the major role of AHL in Sahelian rainfall dynamics, and comparing it with that of SHL, has also led us to discriminate Sahelian rainfall into two indices, "WEST SAHEL" (10˚N-20˚N; 20˚W-10˚W) and
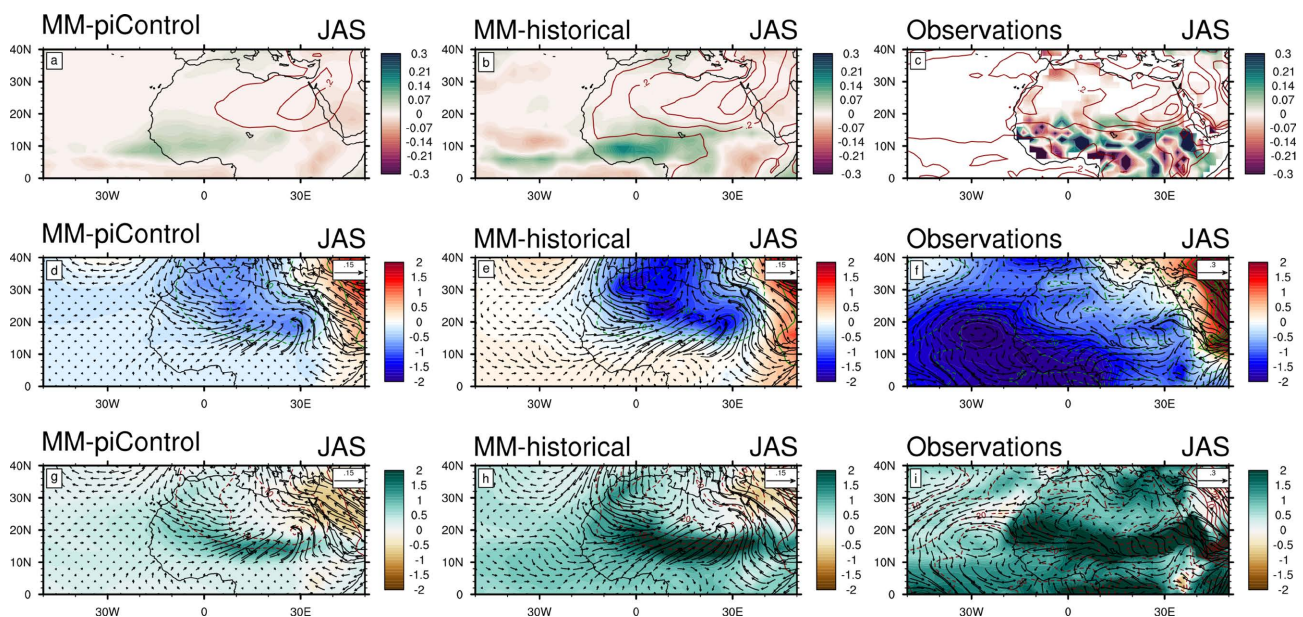

Figure 11. Same as Figure 9 but for AHL index.

"EAST SAHEL" (10˚N-20˚N; 0˚-20˚E). This regionalization also link with several studies highlighting a relative difference in trends between these two zones, in particular over the recent period of partial rainfall recovery from the 1990s onwards. [40] have shown that this recovery is particularly marked in central Sahel, while rainfall shows little change in Senegal zone, inducing, once the general trend over Sahel is eliminated, the emergence of a West/East dipole of precipitation, reminiscent of the RCP8.5 projections [41].

Figure 12 shows the regression maps of 2-meter temperature anomalies and sea level pressure on the standardized precipitation index from three zones (SAHEL, EAST SAHEL and WEST SAHEL). In observations, whatever the precipitation index, the results show a strong structure of positive regression of 2 meters temperatures over the whole of North Africa and the Mediterranean, spilling over the tropical Atlantic Ocean, and globally negative regressions over the whole of the Sahelian strip, indicating higher precipitation. Higher temperatures are associated with zones of lower pressure extending over Saharan zone and tropical Atlantic Ocean. As a result, south-easterly wind anomalies over Atlantic Ocean turn westerly over Sahelian region.

The structures are very similar when we consider the precipitation indices over EAST SAHEL and WEST SAHEL, with a slight shift in longitude of the cold anomalies over Sahelian strip.

In the simulations, the regression fields of control and historical multi-model are similar to each other, with, as is often the case, slightly stronger weights in the historical simulation, which nevertheless remains rather far from observations in terms of temperatures above 20˚N. In these simulations, the impact of Sahelian precipitation on temperatures is clear, as is the difference between the
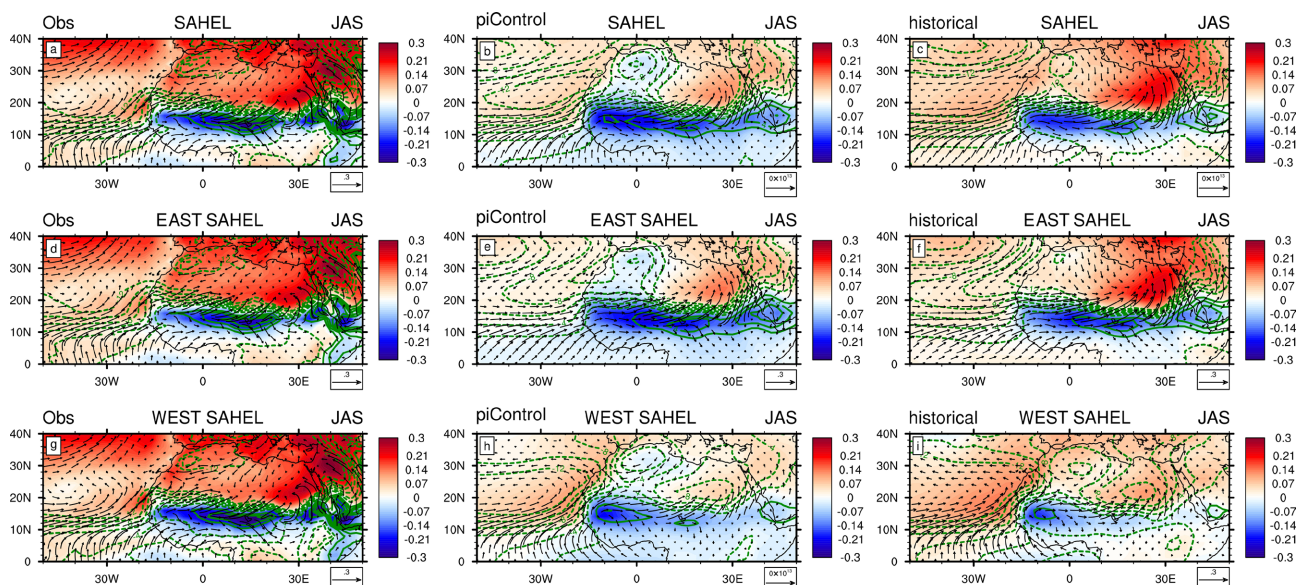
Figure 12. Regression maps of decadal 2 meters air temperature anomalies (colors) and sea level pressure anomalies (green contours) on the decadal precipitation index from 3 zones (SAHEL, EAST SAHEL and WEST SAHEL) for observations and multi-model from 29 CMIP5 models in summer.

index calculated for the western and eastern Sahel. The atmospheric circulation structure is characterized by a strengthening of monsoonal flows, driven on the one hand by a more pronounced cyclonic and low-pressure circulation over the AHL location associated with higher temperatures over Egypt and the eastern Mediterranean, and on the other by another cyclonic and low-pressure circulation over the northern tropical Atlantic at 20°N associated with a meridional temperature gradient, inducing an overall northward rise in ITCZ (see **Figure 12**). The decomposition of Sahelian index into East/West components shows similar structures, with an intensification (weakening) of AHL signal and a weakening (intensification) of the signal over the tropical Atlantic for the East (West) component. In terms of wind, the regression fields show westerly wind anomalies over both the tropical Atlantic and the continent for East Sahel component, and an intensification of southerly winds over the tropical Atlantic and the continent West of the prime meridian for West Sahel component. Consistent with our previous results, there were no anomaly signals at the SHL location.

We then subtracted the AMO signal contribution as in previous sections to analyze the regressions from the residual anomalies. The results are shown in **Figure 13**. In the multi-model average of control simulations, the circulation structures are identical, with a minor weakening. In the multi-model average of the historical simulations, the circulation patterns are also preserved, although with a more pronounced weakening. In the context of the model's internal decadal variability, this once again highlights the independence between oceanic variability modes (in particular AMO) and atmospheric dynamics over the North African continent. Similarly, this independence is less clear-cut in historical simulations, closer to observations, where atmospheric structures, in particular
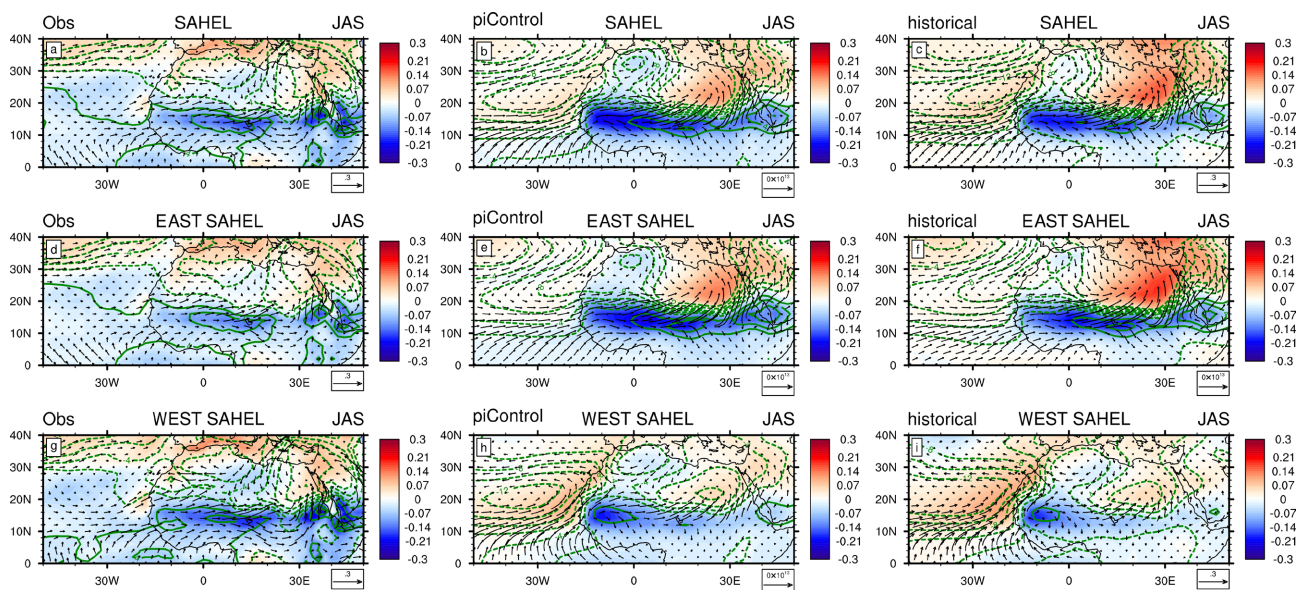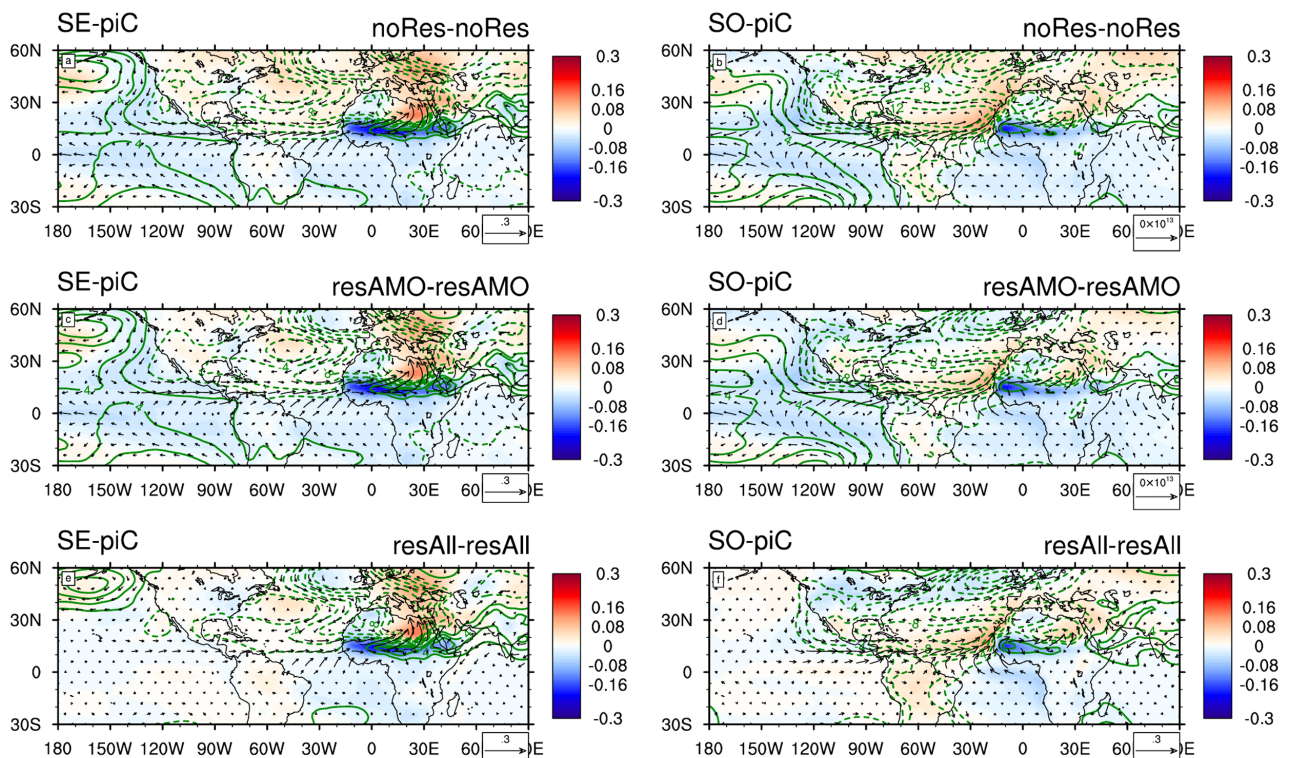

Figure 13. Regression maps of decadal 2 meters air temperature anomalies (colors) and sea level pressure anomalies (green contours) on the decadal precipitation index from 3 zones (SAHEL, EAST SAHEL and WEST SAHEL) for observations, 29 CMIP5 models and the multi-model in summer after subtraction of AMO.

the signal of positive temperature anomalies over North Africa, are strongly modified, confirming the very strong imprint of AMO on the specific relationships between Sahelian precipitation and atmospheric dynamics, linked in particular to AHL via temperature forcing.

Figure 14 shows the same results for the control multi-model average, the reference for internal climate variability, over a wider geographical dimension, while Figure 15 shows the associated results for the precipitation fields. Total regression fields are shown, as well as residual regressions once the influence of AMO has been removed, and then the influence of the three modes (AMO, IPO and IDV) has been removed. Thus, decadal rainfall variability in the Sahel, which appears strongly constrained by AMO in the historical period of observations, is driven mainly in its natural decadal variability, for "East Sahel" zone, by the DTA as well as by an extension of cyclonic circulation over the tropical Atlantic. For "West Sahel" zone, this decadal variability is driven by a meridional dipole structure of sea surface temperature over tropical Atlantic Ocean. In relation to these two rainfall indices, it is worth noting the presence of a meridional precipitation dipole signaling a northward shift of the ITCZ over West Africa and the tropical Atlantic Ocean, with a longitude shift relative to the positioning of these two indices. The extension of the cyclonic circulation over the tropical Atlantic for the "East Sahel" index is reduced quite significantly when the impact

Figure 14. Regression maps of decadal 2 meters air temperature anomalies (colors) and sea level pressure anomalies (green contours) on the decadal precipitation index derived from EAST SAHEL (ES) and WEST SAHEL (WS) for observations and multi-model averaging in summer, without deducting (noRes) oceanic modes (a and d), after deducting (resAMO) AMO (b and e), and after deducting the three (resAll) oceanic modes (c and f).
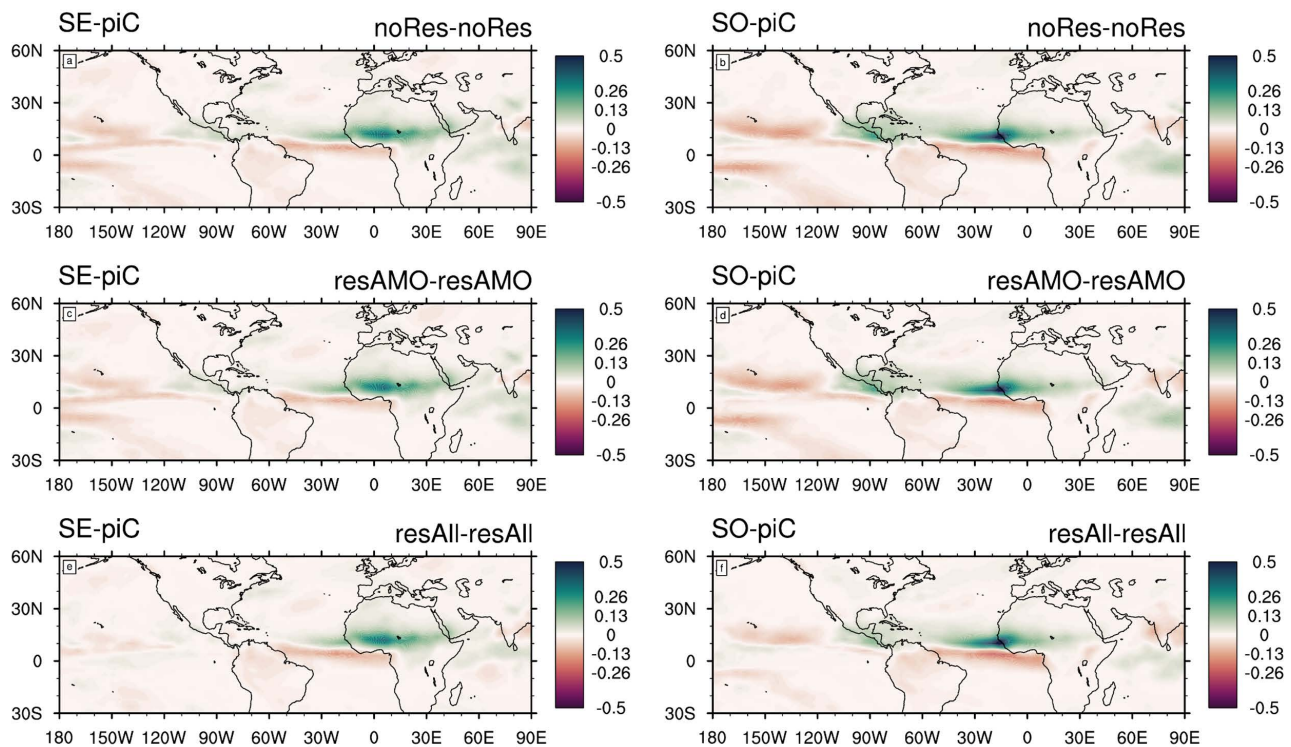
Figure 15. Same as **Figure 14** but for precipitations.

of IPO and IDV is statistically eliminated (but not totally). This may be a numerical artefact, but it may also be a direct effect of IPO. The multi-model showing the impact of IPO on low-level circulation over tropical Atlantic indicates, for a negative phase, a strengthening of this cyclonic extension. AHL thus appears to be a specific factor in decadal rainfall variability over East Sahel zone. However, the footprint of the cyclonic circulation centered on Morocco with a longitude extension over tropical Atlantic is still present, possibly associated with the trace of the inter-hemispheric temperature gradient over tropical Atlantic, which is present even after elimination of AMO footprint. When we switch to the "West Sahel" index, we observe, consistent with this westward shift, a stronger imprint of this inter-hemispheric temperature gradient over the inter-tropical Atlantic, of the associated low-pressure zone over tropical North Atlantic, of the southern component of monsoon winds and of the rainfall dipole over the ocean, and conversely a weaker signal from the cyclonic circulation linked to AHL. These signals over the tropical Atlantic remain strong, even after eliminating the influence of the three oceanic modes.

4. Conclusion

The aim of this study was, on one hand, to analyze decadal and multi-decadal variability of the AMO and, on the other, to assess its influence on the West African Monsoon. At the decadal scale of variability, the analysis show that, over historical period of observations, the AMO has a very strong impact on both Sahelian precipitation and Saharan temperatures and low pressures. Furthermore,

it has been shown that a positive AMO phase induces a rise in temperatures over Sahara and a deepening of SHL and AHL, leading to increased rainfall over Sahel. This results in an overestimated positive correlation between SHL and Sahelian precipitation, which does not reflect the reality of the associated atmospheric dynamics, showing no significant relationship and contradicting many of the results published in the scientific literature. Furthermore, the highlighting of the major role of AHL, whose strengthening favors the transport of moisture flux into the interior of the continent and an excess of precipitation over the entire Sahelian zone, is a new result that emerges from control simulations (reference for the assessment of internal atmospheric variability) and historical simulations, even after eliminating the influence of AMO. This therefore prompts caution in interpretations of decadal-scale relationships between Saharan low-pressure dynamics and AMO. Finally, decadal rainfall variability in the Sahel, once the influence of AMO (and also of the other two modes IPO and IDV) has been eliminated, appears to be driven mainly, for the "East Sahel" zone, by AHL activity, and for the "West Sahel" zone, by the meridional sea surface temperature dipole structure over the tropical Atlantic Ocean.

Acknowledgements

Conflicts of Interest

The authors declare no conflicts of interest regarding the publication of this paper.

References

[1] Sultan, B. and Janicot, S. (2003) The West African Monsoon Dynamics. Part II: The "Preonset" and "Onset" of the Summer Monsoon. *Journal of Climate*, **16**, 3407-3427. https://doi.org/10.1175/1520-0442(2003)016<3407:TWAMDP>2.0.CO;2

[2] Folland, C.K., Palmer, T.N. and Parker, D.E. (1986) Sahel Rainfall and Worldwide Sea Temperatures, 1901-85. *Nature*, **320**, 602-607. https://doi.org/10.1038/320602a0

[3] Janicot, S., Trzaska, S. and Poccard, I. (2001) Summer Sahel-ENSO Teleconnection and Decadal Time Scale SST Variations. *Climate Dynamics*, **18**, 303-320. https://doi.org/10.1007/s003820100172

[4] Lavaysse, C., *et al.* (2009) Seasonal Evolution of the West African Heat Low: A Climatological Perspective. *Climate Dynamics*, **33**, 313-330. https://doi.org/10.1007/s00382-009-0553-4

[5] Mohino, E., Janicot, S. and Bader, J. (2011) Sahel Rainfall and Decadal to Mul-

ti-Decadal Sea Surface Temperature Variability. *Climate Dynamics*, **37**, 419-440. https://doi.org/10.1007/s00382-010-0867-2

[6] Rowell, D.P., Folland, C.K., Maskell, K. and Ward, M.N. (1995) Variability of Summer Rainfall over Tropical North Africa (1906-92): Observations and Modelling. *Quarterly Journal of the Royal Meteorological Society*, **121**, 669-704. https://doi.org/10.1002/qj.49712152311

[7] Thorncroft, C. and Blackburn, M. (1999) Maintenance of the African Easterly Jet. *Quarterly Journal of the Royal Meteorological Society*, **125**, 763-786. https://doi.org/10.1002/qj.49712555502

[8] Lavaysse, C., Flamant, C., Evan, A., Janicot, S. and Gaetani, M. (2015) Recent Climatological Trend of the Saharan Heat Low and Its Impact on the West African Climate. *Climate Dynamics*, **47**, 3479-3498. https://doi.org/10.1007/s00382-015-2847-z

[9] Lavaysse, C., Flamant, C. and Janicot, S. (2010) Regional-Scale Convection Patterns during Strong and Weak Phases of the Saharan Heat Low. *Atmospheric Science Letters*, **11**, 255-264. https://doi.org/10.1002/asl.284

[10] Biasutti, M., Sobel, A.H. and Camargo, S.J. (2009) The Role of the Sahara Low in Summertime Sahel Rainfall Variability and Change in the CMIP3 Models. *Journal of Climate*, **22**, 5755-5771. https://doi.org/10.1175/2009JCLI2969.1

[11] Zhang, R. and Delworth, T.L. (2006) Impact of Atlantic Multidecadal Oscillations on India/Sahel Rainfall and Atlantic Hurricanes. *Geophysical Research Letters*, **33**, L17712. https://doi.org/10.1029/2006GL026267

[12] Knight, J.R. (2005) A Signature of Persistent Natural Thermohaline Circulation Cycles in Observed Climate. *Geophysical Research Letters*, **32**, L20708. https://doi.org/10.1029/2005GL024233

[13] Ting, M., Kushnir, Y., Seager, R. and Li, C. (2011) Robust Features of Atlantic Multi-Decadal Variability and Its Climate Impacts. *Geophysical Research Letters*, **38**, L17705. https://doi.org/10.1029/2011GL048712

[14] Villamayor, J. and Mohino, E. (2015) Robust Sahel Drought Due to the Interdecadal Pacific Oscillation in CMIP5 Simulations. *Geophysical Research Letters*, **42**, 1214-1222. https://doi.org/10.1002/2014GL062473

[15] Zhang, Q., Berntell, E., Li, Q. and Ljungqvist, F.C. (2021) Understanding the Variability of the Rainfall Dipole in West Africa Using the EC-Earth Last Millennium Simulation. *Climate Dynamics*, **57**, 93-107. https://doi.org/10.1007/s00382-021-05696-x

[16] Haarsma, R.J., Selten, F.M., Weber, S.L. and Kliphuis, M. (2005) Sahel Rainfall Variability and Response to Greenhouse Warming. *Geophysical Research Letters*, **32**, L17702. https://doi.org/10.1029/2005GL023232

[17] Liu, Y., Chiang, J.C.H., Chou, C. and Patricola, C.M. (2014) Atmospheric Teleconnection Mechanisms of Extratropical North Atlantic SST Influence on Sahel Rainfall. *Climate Dynamics*, **43**, 2797-2811. https://doi.org/10.1007/s00382-014-2094-8

[18] Martin, E.R., Thorncroft, C. and Booth, B.B.B. (2014) The Multidecadal Atlantic SST—Sahel Rainfall Teleconnection in CMIP5 Simulations. *Journal of Climate*, **27**, 784-806. https://doi.org/10.1175/JCLI-D-13-00242.1

[19] Martin, E.R. and Thorncroft, C.D. (2014) The Impact of the AMO on the West African Monsoon Annual Cycle: Impact of AMO on West African Monsoon. *Quarterly Journal of the Royal Meteorological Society*, **140**, 31-46. https://doi.org/10.1002/qj.2107

[20] Evan, A.T. and Flamant, C. (2014) Water Vapor in the Saharan Heat Low: A Theory

of Interannual to Decadal Scale Variability in the Summertime Circulation over West Africa. https://hal-insu.archives-ouvertes.fr/insu-01183523

[21] Cook, K.H. and Vizy, E.K. (2015) Detection and Analysis of an Amplified Warming of the Sahara Desert. *Journal of Climate*, **28**, 6560-6580. https://doi.org/10.1175/JCLI-D-14-00230.1

[22] Dixon, R.D., Daloz, A.S., Vimont, D.J. and Biasutti, M. (2017) Saharan Heat Low Biases in CMIP5 Models. *Journal of Climate*, **30**, 2867-2884. https://doi.org/10.1175/JCLI-D-16-0134.1

[23] Monerie, P.-A., Pohl, B. and Gaetani, M. (2021) The Fast Response of Sahel Precipitation to Climate Change Allows Effective Mitigation Action. *NPJ Climate and Atmospheric Science*, **4**, Article No. 1. https://doi.org/10.1038/s41612-021-00179-6

[24] Harris, I., Jones, P.D., Osborn, T.J. and Lister, D.H. (2014) Updated High-Resolution Grids of Monthly Climatic Observations—The CRU TS3.10 Dataset. *International Journal of Climatology*, **34**, 623-642. https://doi.org/10.1002/joc.3711

[25] Rayner, N.A. (2003) Global Analyses of Sea Surface Temperature, Sea Ice, and Night Marine Air Temperature since the Late Nineteenth Century. *Journal of Geophysical Research*, **108**, Article No. 4407. https://doi.org/10.1029/2002JD002670

[26] Hersbach, H., Peubey, C., Simmons, A., Berrisford, P., Poli, P. and Dee, D. (2015) ERA-20CM: A Twentieth-Century Atmospheric Model Ensemble. *Quarterly Journal of the Royal Meteorological Society*, **141**, 2350-2375. https://doi.org/10.1002/qj.2528

[27] Titchner, H.A. and Rayner, N.A. (2014) The Met Office Hadley Centre Sea Ice and Sea Surface Temperature Data Set, Version 2: 1. Sea Ice Concentrations. *Journal of Geophysical Research*: *Atmospheres*, **119**, 2864-2889. https://doi.org/10.1002/2013JD020316

[28] Taylor, K.E., Stouffer, R.J. and Meehl, G.A. (2012) An Overview of CMIP5 and the Experiment Design. *Bulletin of the American Meteorological Society*, **93**, 485-498. https://doi.org/10.1175/BAMS-D-11-00094.1

[29] Enfield, D.B., Mestas-Nuñez, A.M. and Trimble, P.J. (2001) The Atlantic Multidecadal Oscillation and Its Relation to Rainfall and River Flows in the Continental U.S. *Geophysical Research Letters*, **28**, 2077-2080. https://doi.org/10.1029/2000GL012745

[30] Wang, C., Dong, S., Evan, A.T., Foltz, G.R. and Lee, S.-K. (2012) Multidecadal Covariability of North Atlantic Sea Surface Temperature, African Dust, Sahel Rainfall, and Atlantic Hurricanes. *Journal of Climate*, **25**, 5404-5415. https://doi.org/10.1175/JCLI-D-11-00413.1

[31] Alexander, M.A., Kilbourne, K.H. and Nye, J.A. (2014) Climate Variability during Warm and Cold Phases of the Atlantic Multidecadal Oscillation (AMO) 1871-2008. *Journal of Marine Systems*, **133**, 14-26. https://doi.org/10.1016/j.jmarsys.2013.07.017

[32] Deser, C. and Phillips, A. (2017) An Overview of Decadal-Scale Sea Surface Temperature Variability in the Observational Record. *Past Global Changes Magazine*, **25**, 2-6. https://doi.org/10.22498/pages.25.1.2

[33] Mann, M.E. (2004) On Smoothing Potentially Non-Stationary Climate Time Series: On Smoothing Climate Time Series. *Geophysical Research Letters*, **31**, L07214. https://doi.org/10.1029/2004GL019569

[34] Dixon, R.D., Vimont, D.J. and Daloz, A.S. (2018) The Relationship between Tropical Precipitation Biases and the Saharan Heat Low Bias in CMIP5 Models. *Climate*

Dynamics, **50**, 3729-3744. https://doi.org/10.1007/s00382-017-3838-z

[35] Monerie, P.-A., Biasutti, M., Mignot, J., Mohino, E., Pohl, B. and Zappa, G. (2023) Storylines of Sahel Precipitation Change: Roles of the North Atlantic and Euro-Mediterranean Temperature. *Journal of Geophysical Research*: *Atmospheres*, **128**, e2023JD038712. https://doi.org/10.1029/2023JD038712

[36] Dalu, G.A., Gaetani, M., Lavaysse, C., Flamant, C., Evan, A.T. and Baldi, M. (2018) Simple Solutions for the Summer Shallow Atmospheric Circulation over North Africa. *Quarterly Journal of the Royal Meteorological Society*, **144**, 765-779. https://doi.org/10.1002/qj.3246

[37] Pu, B. and Cook, K.H. (2010) Dynamics of the West African Westerly Jet. *Journal of Climate*, **23**, 6263-6276. https://doi.org/10.1175/2010JCLI3648.1

[38] Pu, B. and Cook, K.H. (2012) Role of the West African Westerly Jet in Sahel Rainfall Variations. *Journal of Climate*, **25**, 2880-2896. https://doi.org/10.1175/JCLI-D-11-00394.1

[39] Dong, L. and McPhaden, M.J. (2017) Why Has the Relationship between Indian and Pacific Ocean Decadal Variability Changed in Recent Decades? *Journal of Climate*, **30**, 1971-1983. https://doi.org/10.1175/JCLI-D-16-0313.1

[40] Lebel, T. and Ali, A. (2009) Recent Trends in the Central and Western Sahel Rainfall Regime (1990-2007). *Journal of Hydrology*, **375**, 52-64. https://doi.org/10.1016/j.jhydrol.2008.11.030

[41] Biasutti, M. (2013) Forced Sahel Rainfall Trends in the CMIP5 Archive: Forced Rainfall Trends in the Sahel. *Journal of Geophysical Research*: *Atmospheres*, **118**, 1613-1623. https://doi.org/10.1002/jgrd.50206